



## TARGET IMAGE PROCESSING BASED ON SUPER-RESOLUTION RECONSTRUCTION AND MACHINE LEARNING ALGORITHM

CHUNMAO LIU\*

**Abstract.** This article proposes a target image processing method based on super-resolution reconstruction and machine learning algorithms, which solves the low-resolution problem in medical images during imaging. This method uses nonlocal autoregressive learning based on a medical image super-resolution reconstruction method. The autoregressive model is introduced into the sparse representation-based medical image super-resolution reconstruction model by utilizing medical image data inherent nonlocal similarity characteristics. At the same time, a clustering algorithm is used to obtain a classification dictionary, improving experimental efficiency. The experimental results show that ten randomly selected CT/MR images are used as test images, and each image's peak signal-to-noise ratio and structural similarity values are calculated separately. Compared with other methods, the method proposed in this paper is significantly better and can achieve ideal results, with the highest value being 31.49. This method demonstrates the feasibility of using super-resolution reconstruction and machine learning algorithms in medical image resolution.

**Key words:** Medical image, Super-resolution reconstruction, Nonlocal autoregression, Classification dictionary

**1. Introduction.** Many areas of life have high requirements for image resolution, such as security, medical, aerospace, criminal investigation, etc., and image super-resolution reconstruction technology has gradually become a hot topic in recent years. Image super-resolution methods mainly include difference-based, reconstruction-based, and learning-based methods. The difference-based method utilizes the pixel values around a certain pixel point and their relative positional relationships to evaluate mathematical methods, mainly including nearest neighbour interpolation and bicubic interpolation [1]. Reconstruction-based methods mainly use the prior knowledge of natural expectations like smoothness. Common methods include convex set projection and the maximum posteriori probability method. Learning-based methods mainly include traditional machine and deep learning methods, which have been widely used in recent years. Machine learning-based methods generally combine matrix transformation-related methods to learn complex mapping relationships, requiring manual feature extraction for learning. Medical image refers to the use of medical devices to obtain images of internal organs or tissues of a part of the human body without invading the human body to diagnose the patient's condition or conduct medical research [2]. Deep learning is a branch of machine learning and an important means to realize artificial intelligence technology. With the widespread application of deep learning technology in image processing and computer vision, deep learning technology's auxiliary and decision-making role in clinical diagnosis has become a research hotspot in medical image analysis. Intelligent diagnosis of medical images can be roughly divided into three steps. First, obtain a large number of high-quality image data, then preprocess the image, and finally mine the image information for analysis and prediction, as shown in Figure 1.1 [3].

Among them, massive and high-quality image data is the basis of deep learning and training. Image preprocessing, such as registration and region of interest extraction, is the basic guarantee for the accuracy of subsequent analysis. Mining information and establishing prediction models are the keys to clinically intelligent decision-making [4].

**2. Literature Review.** Super-resolution using a convolutional neural network (SRCNN) is the pioneer of deep learning applications in the field of super-resolution and has made a breakthrough in the effect and speed of image super-resolution reconstruction [5]. Many improvements based on SRCNN, which greatly promoted image

---

\* School of Electronics and Information Engineering, Henan Polytechnic Institute, Nan Yang, Henan, China, 473000 (Corresponding author's e-mail: [chunmaoliu3@163.com](mailto:chunmaoliu3@163.com))

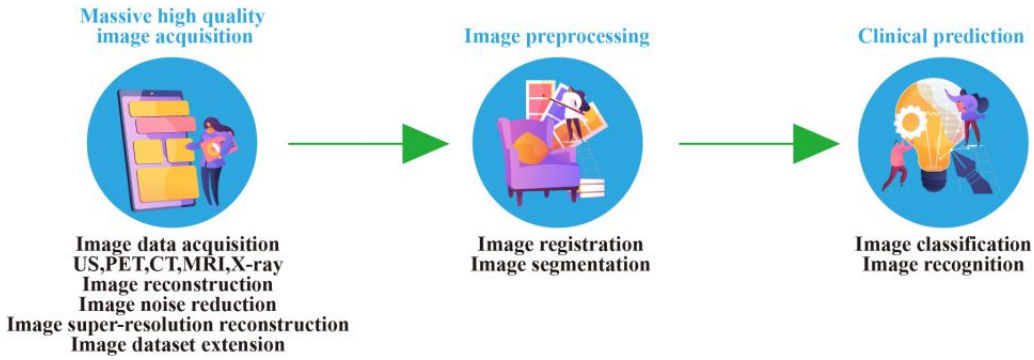


Fig. 1.1: General steps of medical image processing and analysis

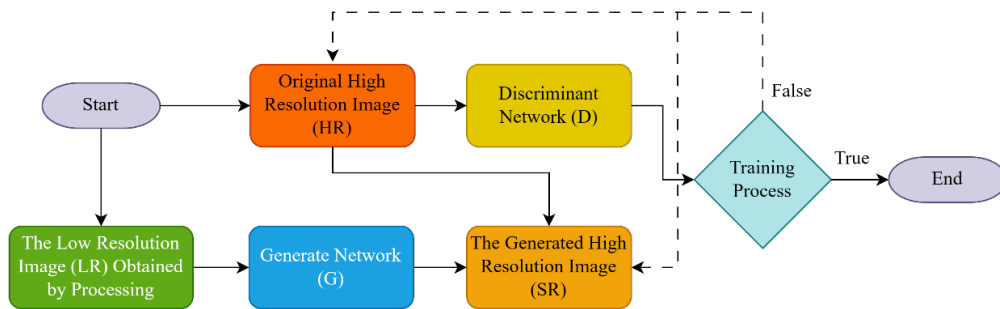


Fig. 2.1: SRGAN training process

super-resolution technology development, are investigated in [6]. After that, the generated countermeasure network is analyzed for image super-resolution reconstruction and the SRGAN algorithm, which makes the image have more high-frequency details and feel better after reconstruction. Still, the training of the Gan network is unstable, and the training time is longer [7]. The training process of SRGAN is shown in Figure 2.1.

The generation network used in SRGAN is a residual network, a dense connection model. Specifically, each layer will accept the previous layer's output as input and the output of all previous layers. The SR reconstruction technology processes one or more low-resolution images to improve the resolution of the original image, compensate for the lost details of LR images, and reconstruct high-resolution (HR) images [8].

An iterative interpolation algorithm is proposed based on curvature after weighing the effect and efficiency of the algorithm and using GPU to accelerate the real-time interpolation of HR images [9]. The learning-based SR algorithm needs to build a learning library by dictionary learning on many HR images to obtain the learning model from LR images to HR images. The authors were inspired by compressed sensing and randomly selected 100,000 image blocks from the training set as samples for training. They also used a sparse coding algorithm to obtain a compact dictionary with many atomic terms [10]. The authors proposed an image SR algorithm using low rank and total variational regularization, which is applied to the SR reconstruction of MR images [11]. A sample learning-based image SR algorithm divides the feature space into multiple subspaces, uses the collected samples to learn the prior information of each subspace, and generates effective mapping functions [12].

**3. Research Methods.** This paper uses a sliding window to divide the image into several overlapping sub-image blocks with a certain step size, as described below.

**3.1. Image similarity characteristics.** After image segmentation, it is usually found that there are many similar structures in these image blocks, and this phenomenon also exists in different images. This

universal similarity can be applied to SR reconstruction of images as a priori information to improve the reconstruction quality of images [13]. When realizing SR reconstruction of medical images, HR images can be obtained by weighting similar image blocks. Therefore, to improve the reconstruction quality of medical images, the constraint of nonlocal similarity of image blocks can be added to the observation model of image super-resolution,  $y = DHx$ . After dividing the image into blocks, take an image block  $x$ , and its nonlocal similar image block.  $x_i^j$  can be weighted to obtain an image block  $x$ , that is

$$x_i \approx \sum_j \omega_i^j x_i^j \quad (3.1)$$

In the experiment, the center of the image block is used to represent the image block  $x_i$ ,  $x_i^j$  is the similar image block of  $x_i$ , and  $\omega_i^j$  is the weighting coefficient of the similar block. When looking for similar image blocks, first use the K-means clustering algorithm to get  $k$  clustering centers. When judging that the image blocks  $x_i^j$  and  $x_i$  are similar, calculate the difference between the current image block  $x_i^j$  and the clustering center  $\hat{x}$  [14].

$$e = \|x_i - \hat{x}\|_2^2 \quad (3.2)$$

The closest image centre from the difference value, and then from this closest cluster is expressed as

$$d_i^j = \|x_i - x_i^j\|_2^2 \leq \theta \quad (3.3)$$

The first  $j$  image blocks most similar to  $x_i$ , where  $\theta$  is the set threshold which is the difference between the  $j^{th}$  image block and  $x_i$ . When  $d_i^j$  is less than the threshold, it is determined that it is a similar image block. Take the first  $j$  image blocks most similar to determine  $\omega_i^j$ :

$$\hat{\omega}_i = \arg \min_{\omega_i} (\|x_i - X\omega_i\|_2^2 + \eta \|\omega_i\|_2^2) \quad (3.4)$$

where  $x$ ,  $\omega_i$ ,  $\eta$  is the regularization coefficient. The purpose of regularization in Equation 3.4 is to improve the stability of the least squares solution. The conjugate gradient method can solve Equation 3.4 to obtain the solution.

$$\hat{\omega}_i = (X^T X + \gamma I)^{-1} X^T x_i \quad (3.5)$$

We use  $\omega_i$  to introduce it into  $x = Sx + e_x$  to build a nonlocal autoregressive model of image  $x$ .  $e_x$  is the model error, while

$$S(i, j) = \begin{cases} \omega_i^j, & \text{If } x_i^j \text{ is a nonlocal similar block of } x_i, \\ 0, & \text{If } x_i^j \text{ is not a nonlocal similar block of } x_i \end{cases} \quad (3.6)$$

A nonlocal autoregressive model is introduced into the SR reconstruction model of sparse images as a new numerical fidelity term to constrain the sparse reconstruction process. Therefore, the SR reconstruction model can be changed to

$$\hat{a} = \arg \min_{\alpha} \{\|y - DS\Psi\alpha\|_2^2 + \gamma \cdot R(\alpha)\} \quad (3.7)$$

$$y = D\psi\alpha \quad (3.8)$$

where  $D$  is the down sampling of the image,  $S$  is the fuzzy kernel function,  $\psi$  is the dictionary,  $\alpha$  is the sparse coefficient of the image block under the dictionary,  $\gamma$  is used to balance the data regularization term, and the data fidelity term and  $R(\alpha)$  is the regularization term. In this way, when the dictionary is trained, dictionary  $\psi$  can be obtained. After entering the input LR image, the sparse coefficient  $\alpha$  corresponding to image  $x$  can be used to reconstruct the HR image using the SR sparse representation model [15,16].

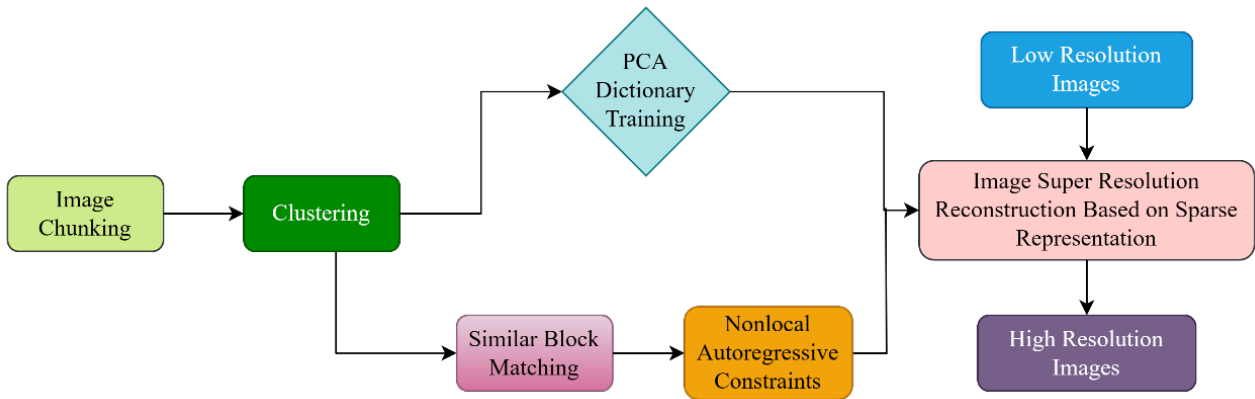


Fig. 3.1: Flow chart super-resolution reconstruction method

**3.2. Medical image super-resolution reconstruction method based on nonlocal autoregressive learning.** The flow chart of the medical image super-resolution reconstruction method based on nonlocal autoregressive learning is proposed and illustrated in Figure 3.1.

**3.2.1. Regularization parameter solution.** In the image SR reconstruction model using sparse representation, the selection of the regularization term  $R(\alpha)$  has a great impact on the reconstruction effect. Generally, using  $l_1$  norm sparse regularization as a constraint, image  $x$  is divided into blocks to obtain image blocks  $x_i, i= 1, 2, \dots, N$ . Each image block can be encoded under dictionary  $\Psi$ . The SR model based on  $l_1$  norm constraint can be rewritten as

$$\hat{\alpha} = \arg \min_{\alpha} \{ \|y - DS\Psi\alpha\|_2^2 + \lambda \sum_{i=1}^N \|\alpha_i\|_1 \} \tag{3.9}$$

$$s.t. y = D\psi\alpha \tag{3.10}$$

where  $\alpha_i$  is the coding vector of the image block  $x_i$ , and the sparse coefficient  $\alpha$  is composed of  $\alpha_i$ . In similar image blocks, image block  $x_i$  can be linearly represented by a similar image block  $x_i^j$ , and the sparse coefficient is closely related to the image block  $x_i$ . For the sparse coefficient  $\alpha_i^j$  corresponding to the similar image block  $x_i^j$ , it should also be closely related to  $\alpha_i$ . Therefore,  $\alpha_i$  should also be very close to the weighted average value of  $\alpha_i^j$ , that is,  $\|\alpha_i - \sum_j \omega_i^j \alpha_i^j\|_2$  should be very small.  $\alpha_i^*$  is used to represent the weighted average value of  $\alpha_i^j$  is given by

$$\alpha_i^* = \sum_j \omega_i^j \alpha_i^j \tag{3.11}$$

Similarly, the super-resolution model is expressed as

$$\hat{\alpha} = \arg \min_{\alpha} \{ \|y - DS\Psi\alpha\|_2^2 + \lambda \|\alpha\|_1 \} \tag{3.12}$$

Add the nonlocal regularization constraint of the above formula to the sparse representation model that is

$$\hat{\alpha} = \arg \min_{\alpha} \{ \|y - DS\Psi\alpha\|_2^2 + \lambda \sum_{i=1}^N \|\alpha_i\|_1 + \eta \sum_{i=1}^N \|\alpha_i - \alpha_i^*\|_2^2 \} \tag{3.13}$$

$$s.t. y = D\psi\alpha \tag{3.14}$$

Since the weighted representation of the normal form can be improved and the sparsity of the formula, the constraint of the normal form is added to the above formula and is given as:

$$\hat{\alpha} = \arg \min_{\alpha} \{ \|y - DS\Psi\alpha\|_2^2 + \sum_{i=1}^N \sum_{j=1}^r \lambda_{i,j} |\alpha_{i,j}| + \sum_{i=1}^N \sum_{j=1}^r \eta_{i,j} (\alpha_{i,j} - \alpha_{i,j}^*)^2 \} \tag{3.15}$$

$$s.t. y = D\psi\alpha \tag{3.16}$$

Rewrite the above formula using Equation 3.15

$$\hat{\alpha} = \arg \min_{\alpha} \{ \|y - DS\Psi\alpha\|_2^2 + \sum_{i=1}^N \|\lambda_i \alpha_i\|_1 + \sum_{i=1}^N \|\eta_i (\alpha_i - \alpha_i^*)\|_2^2 \} \tag{3.17}$$

$$s.t. y = D\psi\alpha \tag{3.18}$$

where  $\lambda_i$  and  $\eta_i$  are diagonal weighting matrices composed of  $\lambda_{i,j}$  and  $\eta_{i,j}$ ,

$$\lambda_{i,j} = \frac{c_1}{|\alpha_{i,j}^{(l)}| + \varepsilon} \tag{3.19}$$

$$\eta_{i,j} = \frac{c_2}{(\alpha_{i,j}^{(l)} - \alpha_{i,j}^*)^2 + \varepsilon} \tag{3.20}$$

$\alpha_{i,j}^{(l)}$  is the value of  $\alpha_{i,j}$ 's  $l$ -th iteration,  $c_1$  and  $c_2$  are preset constants,  $\varepsilon$  is a small positive number used to increase the stability of the above formula.

**3.2.2. Algorithm solution.** The constraint minimization is solved by variable decomposition, and the objective function is mentioned as follows:

$$\begin{aligned} (\hat{x}, \{\hat{\alpha}_i\}) = \arg \min_{x, \{\alpha_i\}} \{ & \|y - DSx\|_2^2 + \beta \sum_{i=1}^N \|R_i x - \psi \alpha_i\|_2^2 + \sum_{i=1}^N \|\lambda_i \alpha_i\|_1 \\ & + \sum_{i=1}^N \|\eta_i (\alpha_i - \alpha_i^*)\|_2^2 \} \end{aligned} \tag{3.21}$$

$$s.t. y = Dx \tag{3.22}$$

Among them,  $R_i$  is used to extract the image block  $x_i$  of the image at  $i$ . if there are enough parameters,  $R_i x_i$  is very close to  $\psi x_i$ , and the objective functions 3.21 and 3.22 are close to equations 3.17 and 3.18.

This paper first clusters the image blocks into  $K$  clusters and learns the PCA Dictionary of each cluster. By introducing  $\psi_k$  into equations 3.21 and 3.22, using an adaptive dictionary, the objective function can be written as

$$\begin{aligned} (\hat{x}, \{\hat{\alpha}_i\}) = \arg \min_{x, \{\alpha_i\}} \{ & \|y - DSx\|_2^2 + \beta \sum_{k=1}^K \sum_{i \in C_k} \|R_i x - \psi_k \alpha_i\|_2^2 + \sum_{i=1}^N \|\lambda_i \alpha_i\|_1 \\ & + \sum_{i=1}^N \|\eta_i (\alpha_i - \alpha_i^*)\|_2^2 \} \end{aligned} \tag{3.23}$$

$$s.t. y = Dx \tag{3.24}$$

Where  $C_k$  is the index set of image blocks in cluster k. Fixed sparsity coefficient  $\{\alpha_i\}$ , x can get the optimal result by minimizing the following Equation:

$$\hat{x} = \arg \min_x \{ \|y - DSx\|_2^2 + \beta \sum_{k=1}^K \sum_{i \in C_k} \|R_i x - \psi_k \alpha_i\|_2^2 \} \quad (3.25)$$

$$s.t. y = Dx \quad (3.26)$$

$$\begin{aligned} \{\hat{\alpha}_i\} = \arg \min_{\{\alpha_i\}} \{ & \beta \sum_{k=1}^K \sum_{i \in S_k} \|R_i x - \psi_k \alpha_i\|_2^2 \\ & + \sum_{i=1}^N \|\lambda_i \alpha_i\|_1 + \eta \sum_{i=1}^N \|\eta_i (\alpha_i - \alpha_i^*)\|_2^2 \} \end{aligned} \quad (3.27)$$

The sparse coefficient  $\{\alpha_i\}$  is obtained.

The above optimization process is iterated until convergence. In the iterative process, the  $\beta$  Makes equations 3.21 and 3.22 better approach equations 3.17 and 3.18. Then, equations 3.25 and 3.26 are solved by using the enhanced Lagrange multiplier (ELM), and equations 3.25 and 3.26 are converted into

$$\begin{aligned} L(x, Z, \mu) = & \|y - DSx\|_2^2 + \beta \sum_{k=1}^K \sum_{i \in C_k} \|R_i x - \psi_k y \alpha_i\|_2^2 + \langle z, y - Dx \rangle \\ & + \mu \|y - Dx\|_2^2 \end{aligned} \quad (3.28)$$

where  $\langle z, y - Dx \rangle$  represents the inner product of z and y-Dx, and Z represents the Lagrange multiplier,  $\mu$  represents a positive scalar. The optimization problems of equations 3.25 and 3.26 can be solved by ALM, which consists of the following iterations:

$$x^{(l+1)} = \arg \min_x L(x, Z^{(l)}, \mu^{(l)}) \quad (3.29)$$

$$Z^{(l+1)} = Z^{(l)} + \mu^{(l)}(y - Dx^{(l+1)}) \quad (3.30)$$

$$\mu^{(l+1)} = \tau \mu^{(l)} \quad (3.31)$$

where  $\tau$  is a constant greater than 1. Fix  $Z^{(l)}$  and  $\mu^{(l)}$ . In the above formula, by making  $\partial L(x, Z^{(l)}, \mu^{(l)}) / \partial x = 0$ , we can derive

$$\begin{aligned} \hat{x}^{(l+1)} = & \left[ (DS)^T DS + \beta \sum_{i=1}^N R_i^T R_i + \mu^{(l)} D^T D \right]^{-1} \\ & \cdot \left[ (DS)^T y + \beta \sum_{i=1}^N R_i^T R_i (\psi_k \alpha_i) + \frac{D^T Z^{(l)}}{2 + \mu^{(l)} D^T D} \right] \end{aligned} \quad (3.32)$$

Because the right inversion matrix of the above formula is large, the conjugate gradient algorithm (CG) is used to calculate X. With the updated estimation of X, it is easy to update Z and  $\mu$ . The process can be iterated until convergence [17].

For the given x, Equation 3.27 is a typical sparse coding problem based on image blocks. For each image block, the sparse coding problem is as follows:

$$\hat{\alpha}_i = \arg \min_{\alpha_i} \{ \beta \|R_i x - \psi_k \alpha_i\|_2^2 + \|\lambda_i \alpha_i\|_1 + \|\eta_i (\alpha_i - \alpha_i^*)\|_2^2 \} \quad (3.33)$$

Table 4.1: PSNR comparison of four methods

Test image	Bicubic Interpolation [18]	Sparse Coding [19]	Quick Method [20]	Proposed Method
No. 1	26.75	28.79	30.67	31.21
No. 2	24.94	28.85	30.81	31.37
No. 3	26.52	27.38	31.35	31.43
No. 4	26.41	30.25	29.11	31.49
No. 5	25.12	28.84	29.59	30.43
No. 6	25.62	27.72	30.77	31.31
No. 7	26.47	29.58	30.63	31.36
No. 8	26.13	27.61	31.09	31.39
No. 9	25.35	28.50	28.47	29.89
No. 10	25.98	28.50	30.38	31.12

To solve the nonlocal regularized sparse coding problem, the iterative shrinkage method is extended from dealing with one  $l_1$  norm constraint to mixed  $l_1$  and  $l_2$  norm constraints. The closed shrinkage function is derived as follows:

$$\hat{\alpha}_{i,j} = \begin{cases} 0, & |v_{i,j}| \leq \frac{\tau_{1,j}}{2\tau_{2,j}+1} \\ v_{i,j} - \text{sign}(v_{i,j}) \frac{\tau_{1,j}}{2\tau_{2,j}+1}, & \text{other} \end{cases} \quad (3.34)$$

where

$$v_{i,j} = \frac{\gamma_{i,j}}{2\tau_{2,j}+1}, \gamma_i = \frac{2\eta_i\alpha_i^*}{\beta} + \psi_k^T R_i x_i \quad (3.35)$$

$$\tau_{1,j} = \frac{\lambda_{i,j}}{\beta}, \tau_{2,j} = \frac{\eta_{i,j}}{\beta}$$

**4. Results and Discussion.** To verify the effect of this method in improving the resolution of medical images, the proposed method is compared with the bicubic interpolation method, sparse coding-based method (SC), and fast direct super-resolution method. This paper uses the real CT/MR images provided by TCIA and LIDC in the experiment, and the test images are randomly selected.

Some parameters need to be present in the actual experiment. The image block size is set to  $5 \times 5$ . The step size is 2. Number of clusters  $K = 60$ ,  $\gamma = 42000$ ,  $\mu^{(0)} = 1.4$ ,  $\tau = 1.2$ ,  $\beta^{(0)} = 0.1$ ,  $\rho = 2$ ,  $\lambda$  and  $\eta$  balance sparse regularization and data fidelity terms. Initialization, when calculating the adaptive regularization parameters  $\lambda_i$  and  $\eta_i$ , it is necessary to set the values of  $c_1$  and  $c_2$ . Through repeated experiments, this paper sets,  $c_1 = 0.25$  and  $c_2 = 3.6$  to balance the operation speed and visual effect.

In the data set of this paper, 10 CT/MR images are randomly selected as test images. Each image's peak signal-to-noise ratio (PSNR) value and structural similarity (SSIM) value are calculated and compared with other existing methods. Table 4.1 shows the comparison of PSNR with other conventional methods. Figure 4.1 and Figure 4.2 show the comparison results of corresponding PSNR and SSIM values, respectively.

It can be seen from the chart that the PSNR value and SSIM value of the proposed method are higher, which are more similar to the original HR image. The proposed method has achieved satisfactory results in SR reconstruction of medical images.

**5. Conclusion.** This paper proposes a target image processing based on super-resolution reconstruction and a machine learning algorithm. Starting from the sparse representation, this paper introduces the existence of similar image structures in medical images. The self-similarity characteristics of medical images are added to the sparse representation theory of images, and the PCA dictionary learning is used to complete the SR reconstruction process of medical images. Experimental analysis is conducted through subjective visual judgment and objective data comparison. From the experimental results, it can be seen that the reconstruction effect

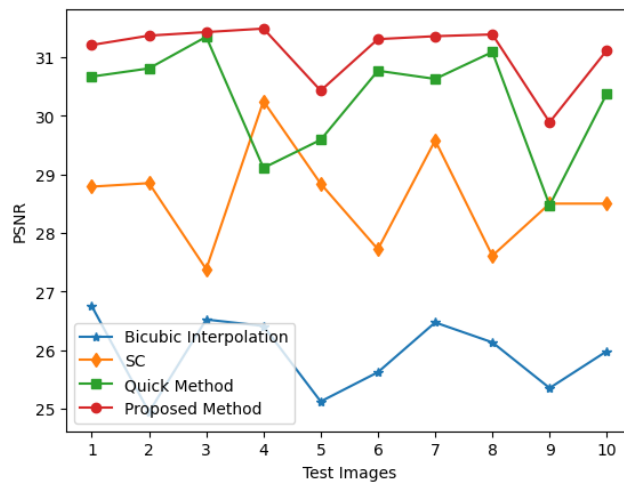


Fig. 4.1: PSNR Comparison of three models with the proposed method

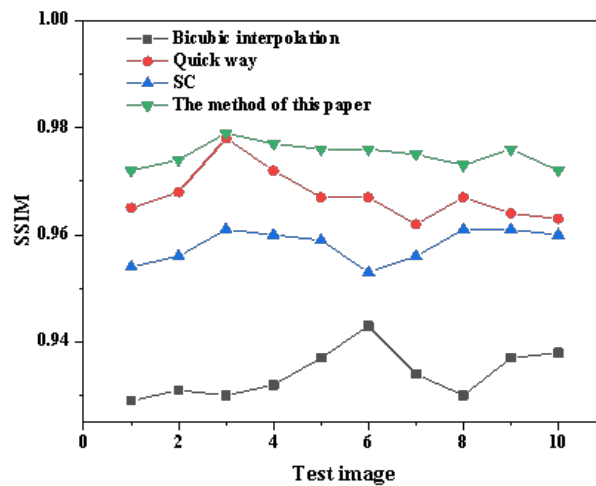


Fig. 4.2: SSIM Comparison of three models with the proposed method

of this method is good. In addition, this paper first clusters the images and significantly reduces the time of querying similar image blocks. The proposed method exhibits a long running time if the number of datasets is huge.

REFERENCES

[1] Junrui, X., Yutan, W., Aili, Q., Jiaxin, Z., Zhenwei, X., Haiyan, W., & Haowei, S. (2021). Image segmentation method for Lingwu long jujubes based on improved FCN-8s [J]. Transactions of the Chinese Society of Agricultural Engineering (Transactions of the CSAE), 37(5), 191-197.

[2] Liu, B. , & Chen, J. . (2021). A super resolution algorithm based on attention mechanism and SRGAN network. IEEE Access, PP(99), 1-1.

- [3] McAuliffe, M. J., Lalonde, F. M., McGarry, D., Gandler, W., Csaky, K., & Trus, B. L. (2001, July). Medical image processing, analysis and visualization in clinical research. In Proceedings 14th IEEE Symposium on Computer-Based Medical Systems. CBMS 2001 (pp. 381-386). IEEE.
- [4] Jin, W., Li, X., Fatehi, M., & Hamarneh, G. (2023). Guidelines and evaluation of clinical explainable AI in medical image analysis. *Medical Image Analysis*, 84, 102684.
- [5] Li, K., Yang, S., Dong, R., Wang, X., & Huang, J. (2020). Survey of single image super-resolution reconstruction. *IET Image Processing*, 14(11), 2273-2290.
- [6] Zhang, S., Liang, G., Pan, S., & Zheng, L. (2018). A fast medical image super resolution method based on deep learning network. *IEEE Access*, 7, 12319-12327.
- [7] Zhu, Y., Zhou, Z., Liao, G., & Yuan, K. (2020, April). CsrGAN: medical image super-resolution using a generative adversarial network. In 2020 IEEE 17th International Symposium on Biomedical Imaging Workshops (ISBI Workshops) (pp. 1-4). IEEE.
- [8] Zhang, K., Tao, D., Gao, X., Li, X., & Xiong, Z. (2015). Learning multiple linear mappings for efficient single image super-resolution. *IEEE Transactions on Image Processing*, 24(3), 846-861.
- [9] Bhatti, U. A. , Yu, Z. , Yuan, L. , Nawaz, S. A. , & Wen, L. . (2020). Geometric algebra applications in geospatial artificial intelligence and remote sensing image processing. *IEEE Access*, PP(99), 1-1.
- [10] Bao, C., Ji, H., Quan, Y., & Shen, Z. (2015). Dictionary learning for sparse coding: Algorithms and convergence analysis. *IEEE transactions on pattern analysis and machine intelligence*, 38(7), 1356-1369.
- [11] Xiao, Z., Du, N., Liu, J., & Zhang, W. (2021). SR-Net: a sequence offset fusion net and refine net for undersampled multislice MR image reconstruction. *Computer Methods and Programs in Biomedicine*, 202, 105997.
- [12] Zhang, H., Zhang, L., & Shen, H. (2012). A super-resolution reconstruction algorithm for hyperspectral images. *Signal Processing*, 92(9), 2082-2096.
- [13] Niu, X. (2018, December). An overview of image super-resolution reconstruction algorithm. In 2018 11th International Symposium on Computational Intelligence and Design (ISCID) (Vol. 2, pp. 16-18). IEEE.
- [14] Katkar, J., Baraskar, T., & Mankar, V. R. (2015, October). A novel approach for medical image segmentation using PCA and K-means clustering. In 2015 International Conference on Applied and Theoretical Computing and Communication Technology (iCATccT) (pp. 430-435). IEEE.
- [15] Zhao, H. , Liu, Y. , Huang, C. , & Wang, T. . (2020). Hybrid-weighted total variation and nonlocal low-rank based image compressed sensing reconstruction. *IEEE Access*, PP(99), 1-1.
- [16] Fayez, M., Safwat, S., & Hassanein, E. (2016, July). Comparative study of clustering medical images. In 2016 SAI Computing Conference (SAI) (pp. 312-318). IEEE.
- [17] Zha, Z. , Yuan, X. , Zhou, J. , Zhu, C. , & Wen, B. . (2020). Image restoration via simultaneous nonlocal self-similarity priors. *IEEE Transactions on Image Processing*, PP(99), 1-1.
- [18] Triwijoyoa, B. K., & Adila, A. (2021). Analysis of medical image resizing using bicubic interpolation algorithm. *J. Ilmu Komput*, 14(2), 20-29.
- [19] Zhang, R., Shen, J., Wei, F., Li, X., & Sangaiah, A. K. (2017). Medical image classification based on multi-scale non-negative sparse coding. *Artificial intelligence in medicine*, 83, 44-51.
- [20] Zhang, S., Liang, G., Pan, S., & Zheng, L. (2018). A fast medical image super resolution method based on deep learning network. *IEEE Access*, 7, 12319-12327.

*Edited by:* Venkatesan C

*Special issue on:* Next Generation Pervasive Reconfigurable Computing for High Performance Real Time Applications

*Received:* Sep 27, 2023

*Accepted:* Feb 8, 2024